inorganics

MDPI

Article

The Flower-like Co_3O_4 Hierarchical Microspheres for Methane Catalytic Oxidation

Changpeng Lv [1], Dan Du [2], Chao Wang [2,3,*], Yingyue Qin [1], Jinlong Ge [1], Yansong Han [1], Junjie Zhu [1] and Muxin Liu [1,*]

[1] Anhui Provincial Engineering Laboratory of Silicon-Based Materials, School of Materials and Chemical Engineering, Bengbu University, Bengbu 233030, China; lvcp1213@gmail.com (C.L.); qinyingyue@126.com (Y.Q.); jinlongge2005@126.com (J.G.); hanyansozai@163.com (Y.H.); 2121011388@ahnu.edu.cn (J.Z.)

[2] Yankuang Technology Co., Ltd., Shandong Energy Group Co., Ltd., Jinan 250101, China; danya121@163.com

[3] College of Chemical Engineering, Qingdao University of Science and Technology, Qingdao 266042, China

* Correspondence: wangchao5923@hotmail.com (C.W.); liumx49@163.com (M.L.)

Abstract: The development of non-noble Co_3O_4 catalysts exposing highly active crystal planes to low-temperature methane oxidation is still a challenge. Hence, a facile solvothermal method was adapted to construe flower-like Co_3O_4 hierarchical microspheres (Co_3O_4-FL), which are composed of nanosheets with dominantly exposed {112} crystal planes. The flower-like hierarchical structure not only promotes the desorption of high levels of active surface oxygen and enhances reducibility, but also facilitates an increase in lattice oxygen as the active species. As a result, Co_3O_4-FL catalysts offer improved methane oxidation, with a half methane conversion temperature (T_{50}) of 380 °C (21,000 mL g^{-1} h^{-1}), which is much lower than that of commercial Co_3O_4 catalysts (Co_3O_4-C). This study will provide guidance for non-noble metal catalyst design and preparation for methane oxidation and other oxidative reactions.

Keywords: flower-like; tricobalt tetroxide; methane; oxidation

check for updates

Citation: Lv, C.; Du, D.; Wang, C.; Qin, Y.; Ge, J.; Han, Y.; Zhu, J.; Liu, M. The Flower-like Co_3O_4 Hierarchical Microspheres for Methane Catalytic Oxidation. *Inorganics* **2022**, *10*, 49. https://doi.org/10.3390/inorganics10040049

Received: 26 January 2022
Accepted: 29 March 2022
Published: 2 April 2022

Publisher's Note: MDPI stays neutral with regard to jurisdictional claims in published maps and institutional affiliations.

Copyright: © 2022 by the authors. Licensee MDPI, Basel, Switzerland. This article is an open access article distributed under the terms and conditions of the Creative Commons Attribution (CC BY) license (https://creativecommons.org/licenses/by/4.0/).

1. Introduction

The emission of volatile organic compounds (VOCs) is a global environmental issue related to atmospheric pollution and is harmful to human health and the environment due to toxic and/or carcinogenic smog and greenhouse gasses. Thus, it is necessary to develop various methods to eliminate VOCs, including incineration, catalytic removal, adsorption, absorption, condensation, and biofiltration, among which catalytic oxidation is regarded as the most efficient process, and it is especially effective in addressing low concentrations of VOCs [1,2].

Methane, with ultralow concentrations in air, is a highly chemically stable compound, with the highest C–H bond energy of ~435 kJ mol^{-1} in its hydrocarbons, and it has 28~36 times the greenhouse effect of carbon dioxide [3]. Therefore, designed catalysts should be capable of the catalytic oxidation of methane, with a high activity, low catalytic temperature and excellent selectivity for carbon dioxide. Before now, the catalysts for methane have been divisible into noble metal and transition metal oxides. The former achieves high catalytic performance at low temperatures; however, they are expensive, and prone to deactivation. The latter have high potential activity, low costs and thermal stability [4,5].

Among the transition metal oxide catalysts, Co_3O_4 has attracted wide attention for the catalytic oxidation of VOCs (methane, toluene, n-hexanal), given its different potential morphologies, its spinel structure with strong Co^{3+}/Co^{2+} redox properties, and its unique exposed crystal planes [6–11].

Studies have shown that Co_3O_4 nanosheets exhibit high catalytic activity, despite their lower special surface area compared with Co_3O_4 nanobelts and nanocubes [12]. The main reason for the different capacity for catalytic oxidation shown by methane is that the {112} exposed planes of nanosheets are more reactive than the exposed planes in the other morphologies, due to the low energy required for breaking the C–H bond [13]. Meanwhile, Co_3O_4 nanotubes also present better catalytic activity than Co_3O_4 nanorods and nanoparticles during methane oxidation, which is not only related to the presence of {112} exposed planes, but also its open structure [14]. Nevertheless, using lattice oxygen as the active species and the presence of defects should induce the improvement of catalytic activity [15].

The objective of this work is to study the preparation of flower-like Co_3O_4 (FL) hierarchical microspheres stacked with mass nanosheets via a simple solvothermal method and to examine its catalytic activity for methane oxidation. The as-synthesized Co_3O_4-FL was characterized by N_2 physisorption, X-ray diffraction (XRD), field-emission scanning electron microscopy (SEM), transmission electron microscopy (TEM), X-ray photoelectron spectroscopy (XPS), H_2 temperature-programmed reduction (H_2-TPR) and O_2 temperature-programmed desorption (O_2-TPD) in order to investigate the physical-chemical properties. The enhanced catalytic performance can be attributed to the highly exposed {112} planes of the nanosheets, together with the active lattice oxygen and derivative oxygen vacancies on their surfaces.

2. Experimental

2.1. Co_3O_4-FL Preparation

All reagents were purchased from Aladdin Co., Ltd. (Shanghai, China) and used without further purification. In a typical procedure, 2 mmol $CoCl_2$ and 0.01 g polyvinyl alcohol (PVA) was dissolved with stirring for 30 min in a 30 mL mixture of deionized water and ethylene glycol, with a volume ratio of 2:1, to form a homogeneous solution, and then the solution was transferred into a 50 mL Teflon-lined stainless-steel autoclave and maintained at 180 °C for 24 h. After cooling to room temperature, the precipitate was then collected by centrifugation and washed with deionized water and ethanol several times, then dried in an oven at 60 °C overnight to obtain the $Co(OH)_2$ precursor. Co_3O_4-FL was obtained by calcining the as-prepared precursor at 450 °C for 2 h in air. The commercial Co_3O_4 (Co_3O_4-C) was made from agglomerate nanoparticles with grain sizes of 30 nm on a micro scale, which were provided for comparison by Aladdin Co., Ltd. (Shanghai, China). In a typical procedure, the precipitate of the $Co(OH)_2$ precursor collected after the solvothermal process is approximately 0.15 g. The mass of the final Co_3O_4-FL after calcining is about 0.13 g. Both the Co_3O_4-FL and Co_3O_4-C were utilized directly as catalysts for methane oxidation without further treatment.

2.2. Characterizations

The X-ray diffraction (XRD) pattern of the catalyst was determined on a Bruker D8 diffractometer (Billerica, MA, USA) with Cu Kα radiation (λ = 0.154184 nm). Scanning electron microscopy (SEM) was performed on an FEI Inspect F50 microscope (Hillsboro, OR, USA), while transmission electron microscopy (TEM) was performed on an FEI Tecnai F30 microscope (Hillsboro, OR, USA). The specific surface areas were measured at liquid nitrogen temperature using a ASAP2020 Micromeritics instrument (Norcross, GA, USA). Specific surface areas of the samples were calculated using the BET equation. The hydrogen temperature-programmed reduction (H_2-TPR) was performed on a Quantachrome Chembet Pulsar (Boynton Beach, FL, USA) using 10 vol.% H_2/Ar (50 mL·min^{-1}) as the reducing gas. The reduction temperature increased from 50 to 600 °C at a rate of 10 °C·min^{-1}. The oxygen temperature-programmed desorption (O_2-TPD) experiment was performed on a Quantachrome Chembet Pulsar (Boynton Beach, FL, USA). Firstly, 100 mg of catalyst was pretreated in a 3 vol.% O_2/He flow at 450 °C for 30 min. After cooling to 50 °C under the same oxidative atmosphere, the catalyst was purged by a stream of puri-

fied He (30 mL·min^{-1}). Then, the reactor was heated up to 600 °C at an increasing rate of 10 °C·min^{-1}. X-ray photoelectron spectroscopy (XPS) analysis was carried out on a Thermo Fisher ESCALAB 250Xi spectrometer (Waltham, MA, USA) using an Al Kα (1486.6 eV) radiation source. The binding energy of the C 1s electron (284.6 eV) was used to calibrate the spectra.

2.3. Catalytic Tests

The methane oxidation reaction was performed on a fixed bed reactor operated with 0.1 g of catalysts at atmospheric pressure. The reactant gas consisted of 2 vol.% of CH_4, 20 vol.% of O_2 and 78 vol.% of Ar passed through the catalysts with a gas flow rate of 35 mL min^{-1}, which corresponds to a weight hourly space velocity (WHSV) of 21,000 mL·g^{-1}·h^{-1}. The reaction temperature was raised from 50 to 550 °C at a rate of 2 °C·min^{-1}. The reactant and products were analyzed online with a gas chromatograph (Shimadzu, GC-2014, Kyoto, Japan) equipped with a flame ionization detector (FID) and a chromatographic column (GDX 502, 2 m × 3 mm). The conversion of methane was determined every 30 °C with the following equation:

$$CH_4 \text{ conversion } (\%) = (1 - [CH_4]_{out}/[CH_4]_{in}) \times 100 \quad (1)$$

3. Results and Discussion

3.1. Catalytic Characterization

The XRD patterns of the as-prepared precursors $Co(OH)_2$, Co_3O_4-FL, and Co_3O_4-C are presented in Figure 1. The diffraction peaks of Co_3O_4-FL observed at 19.0, 31.3, 36.9, 38.5, 44.8, 55.7, 59.3 and 65.2° can be assigned to the (111), (220), (311), (222), (400), (422), (511) and (440) lattice planes of the Co_3O_4 phase (JCPDS NO.43-1003), respectively. The Co_3O_4-FL was prepared from the as-prepared $Co(OH)_2$ precursor, which was formed through the hydrothermal method from $CoCl_2$ and PVA. All the diffraction peaks can be assigned to $Co(OH)_2$, in agreement with the standard diffraction file (JCPDS No. 30-0443). After calcination, no other peaks suggesting impurities were found in the XRD pattern of the Co_3O_4-FL, which indicates that the $Co(OH)_2$ precursor was completely transitioned into Co_3O_4 without any impurities. Co_3O_4-C was also identified without any impurities by XRD analysis. Nevertheless, there are obvious differences in the specific surface areas of Co_3O_4-FL and Co_3O_4-C catalysts, which were 22 and 12 m^2·g^{-1}, respectively.

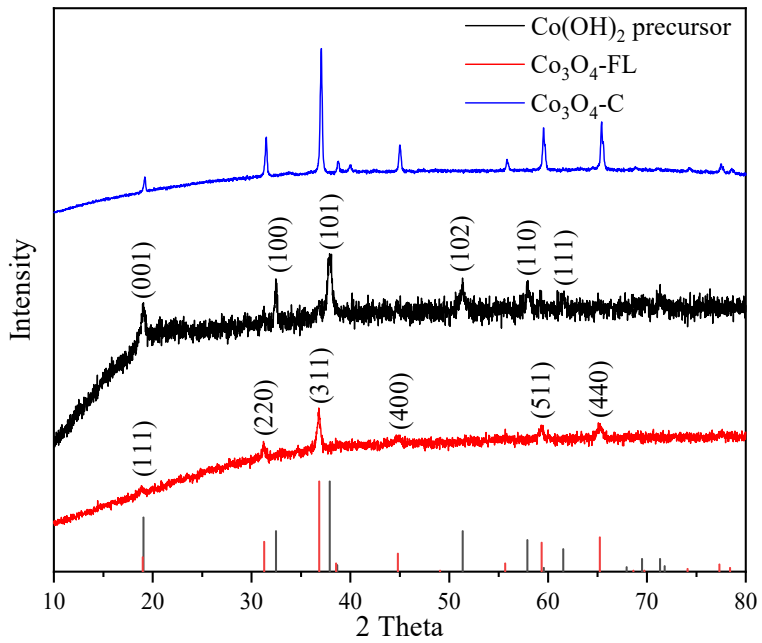

Figure 1. XRD patterns of the as-prepared $Co(OH)_2$ precursor, Co_3O_4-FL, and Co_3O_4-C.

Figure 2 shows the SEM and high-resolution (HR)TEM images of the Co_3O_4-FL and Co_3O_4-C. Figure 2a shows that most Co_3O_4-FLs are monodispersed microspheres with a diameter size of 10–15 µm. Closer observations show that these hierarchical microspheres are composed of large numbers of nanosheets with smooth surfaces (Figure 2b,c). The HRTEM image of the Co_3O_4-FL is presented in Figure 2d. The dominant exposed planes are {112}, which are the only planes displayed in both the set of (220) planes with a lattice space of 0.288 nm and the set of (311) planes with a crossing lattice space of 0.245 nm [16]. Co_3O_4-C, on the other hand, has no definite shape, and just agglomerates nanoparticles (Figure 2e,f).

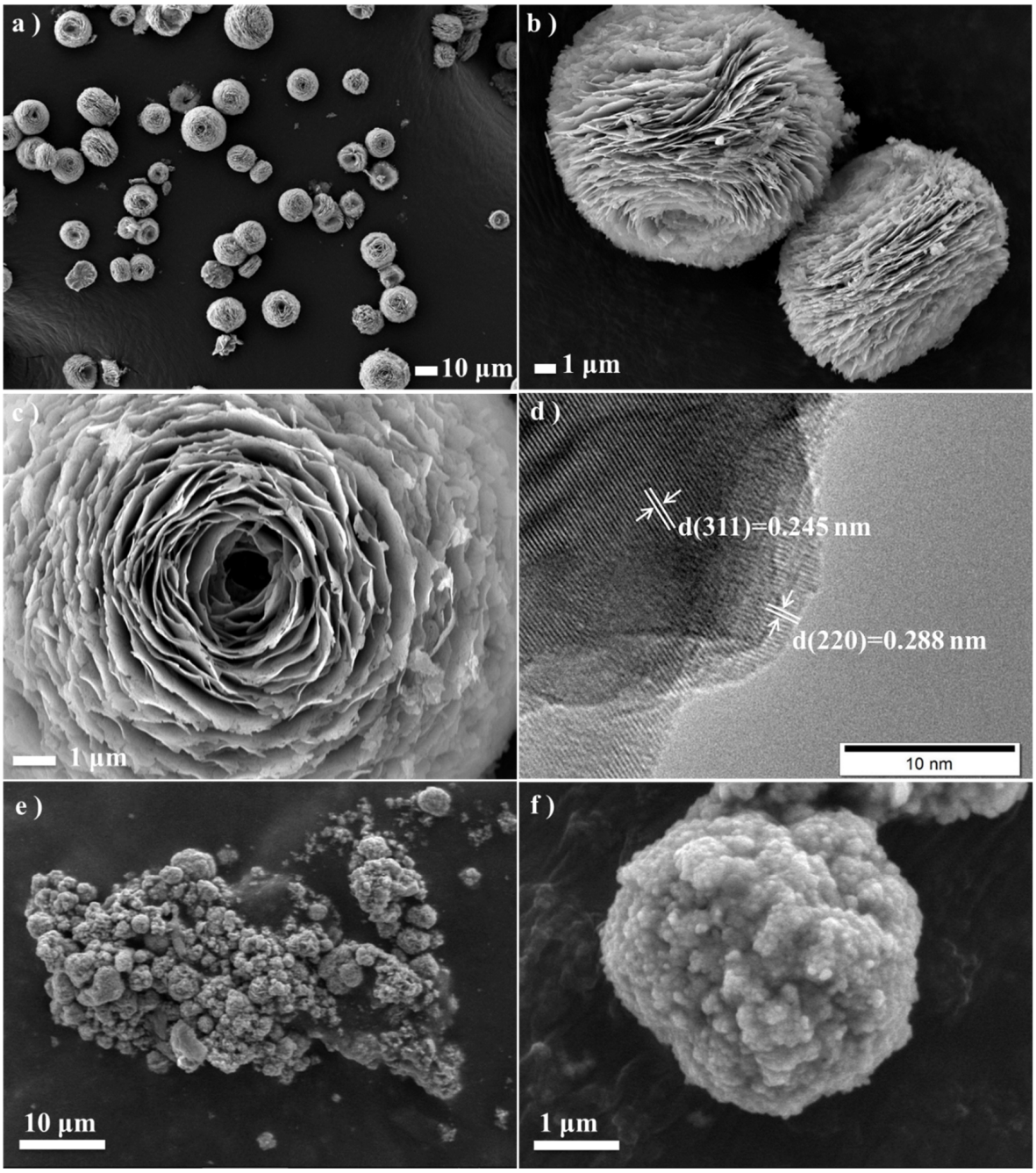

Figure 2. SEM images of the Co_3O_4-FL catalysts at low (**a**) and high (**b**,**c**) magnifications, TEM image of the Co_3O_4-FL catalysts (**d**), and SEM images of the Co_3O_4-C catalysts at low (**e**) and high (**f**) magnifications.

The H_2-TPR profiles show two reduction peaks on both the Co_3O_4-FL and the Co_3O_4-C catalysts (Figure 3). This figure shows overlapping peaks at 385 and 435 °C, observed on Co_3O_4-C, which are assigned to the reduction of Co^{3+} into Co^0. However, there are two peaks in the Co_3O_4-FL catalyst at 342 and 406 °C, indicating the successive reduction behavior of Co^{3+} to Co^{2+} and Co^{2+} to Co^0, in two reduction steps. Additionally, the temperature of the reduction peaks over Co_3O_4-FL is lower than that over Co_3O_4-C, which could imply that the Co_3O_4-FL composed of nanosheets presents the better reducibility, whereby the more susceptible to reduction an oxide is, the more easily it can generate oxygen vacancies [17].

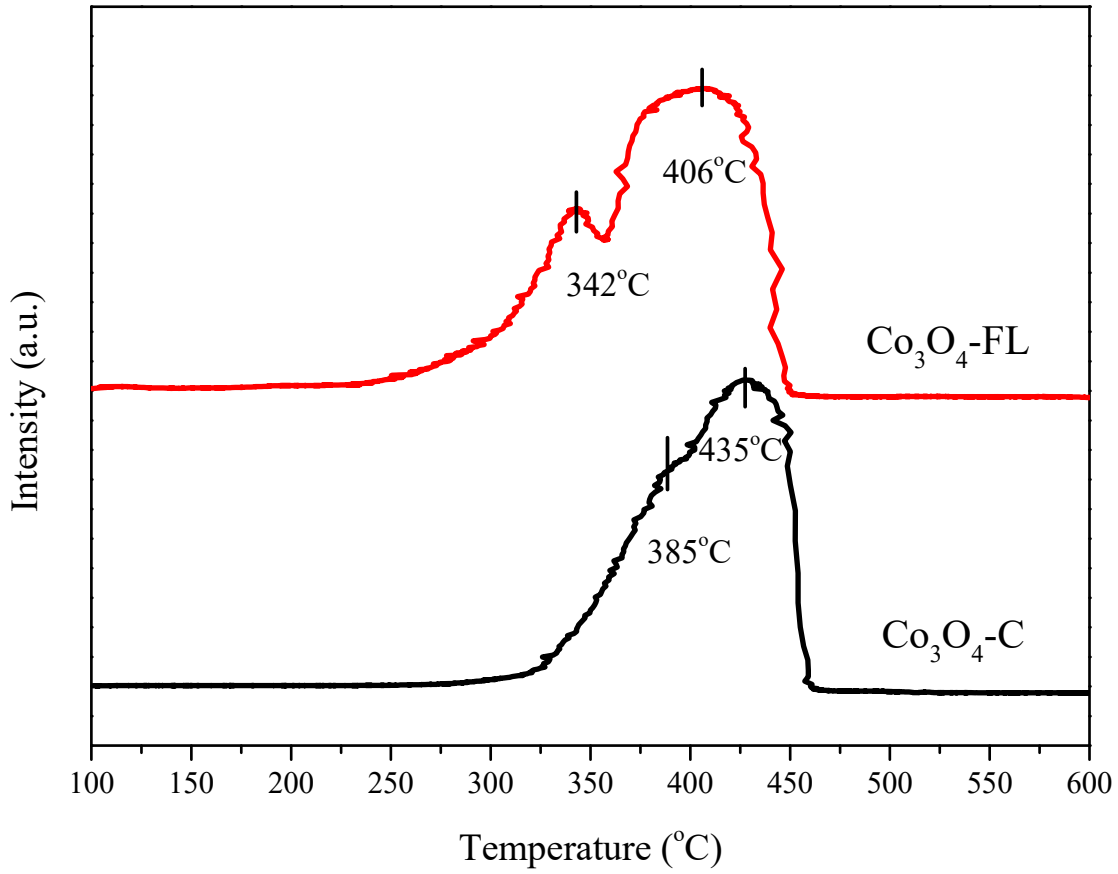

Figure 3. H_2-TPR profiles of the Co_3O_4-FL and Co_3O_4-C catalysts.

The O_2-TPD of catalysts was carried out to evaluate the mobility of oxygen species, as shown in Figure 4. Generally, there are four oxygen species on the surfaces of metal oxides, with the release order: O_2 (molecular oxygen) → O^{2-} (superoxide anion) → O^- (oxygen anion) → O^{2-} (lattice oxygen). The physically adsorbed O_2 species can be desorbed below 200 °C. The O^{2-} and O^- species are chemically adsorbed oxygen, which can be liberated in the range of 200–400 °C. The rest of the O^{2-} species are attributed to surface and/or lattice oxygen released above 400 °C [18]. It seems that the Co_3O_4-FL catalysts present desorption peaks at 206 and 345 °C, which can be attributed to the desorption of O_2^- and O^- species, respectively, whereas another peak is located at 415 °C, which can be assigned to the desorption of O^{2-} species. The desorption temperature of the Co_3O_4-C catalysts shifts from 206 to 257 °C, and from 415 to 482 °C, respectively, indicating that the desorption of O_2^-, O^-, and O^{2-} species was facilitated, implying an enhancement in the catalytic activity of Co_3O_4-FL through a suprafacial mechanism.

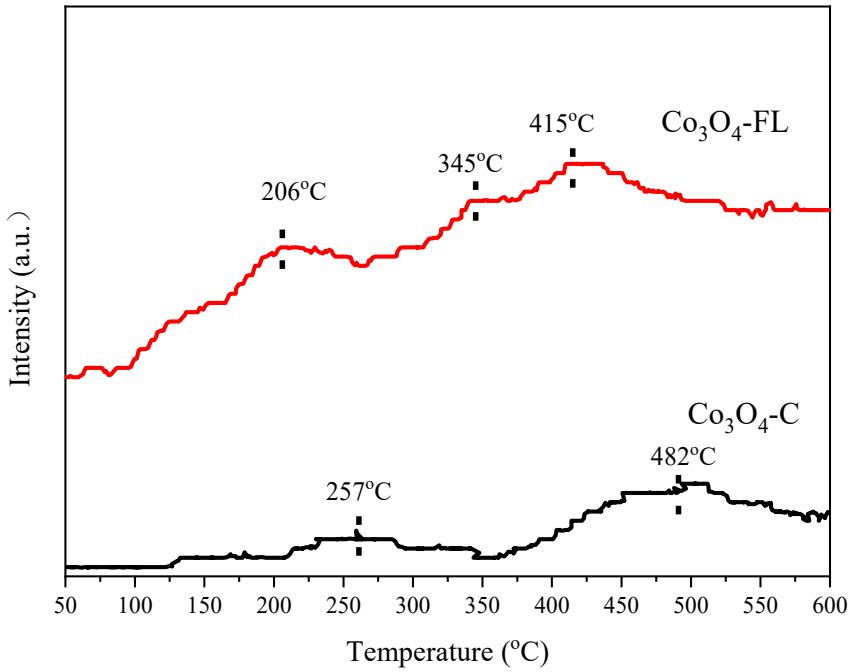

Figure 4. O_2-TPD profiles of the Co_3O_4-FL and Co_3O_4-C catalysts.

The spectra of Co 2p and O 1s are displayed in Figure 5a,b, illustrating the chemical surface compositions and valence states. The BE value of Co $2p_{3/2}$ is 779–780 eV, and a $2p_{1/2}$ splitting of 15 eV is characteristic of the octahedral Co^{3+} component of Co_3O_4 [19]. The satellite peaks at 785 eV evidence the existence of Co^{2+} species in the octahedral sites [20,21]. Here, the Co 2p spectra were resolved using a fitting procedure partially based on that suggested by Biesinger et al. [22]. The contributions of the Co^{3+} and Co^{2+} cations can be identified at 779.5 and 781.1 eV, respectively [23]. Additionally, two satellite peaks, S_1 and S_2, at 785.3 and 789.4 eV, appeared due to electron correlations and the final state effects in the Co^{2+} and Co^{3+} cations, respectively [24]. Meanwhile, the satellite peak S_3 indicates the spin orbit contributions of Co $2p_{1/2}$, as do the satellites S_1 and S_2 [25,26]. The O 1s spectra in Figure 5b are also decomposed into two peaks. The peaks located at 529.7 and 531.2 eV can be ascribed to lattice oxygen (O_{latt}, i.e., O^{2-}) and oxygen adsorbed onto the surface oxygen vacancies (O_{sur}, i.e., O^-, O_2^{2-}, and OH^-), respectively [27].

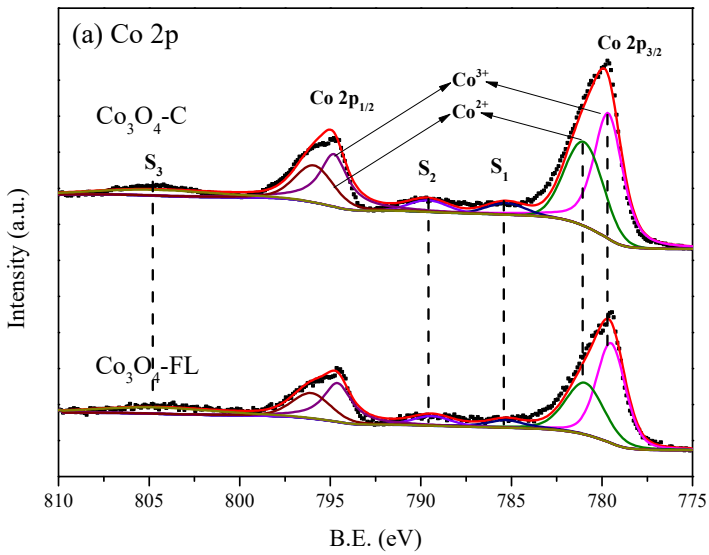

Figure 5. *Cont.*

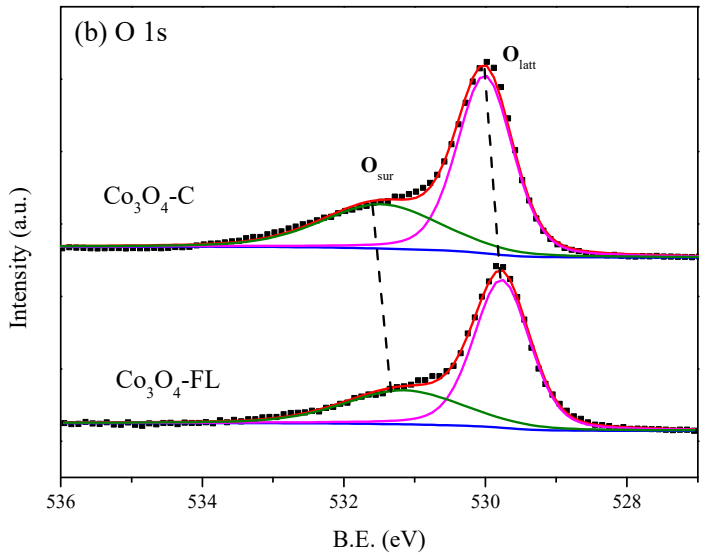

Figure 5. (**a**) Co 2p and (**b**) O 1s XPS spectra of the Co_3O_4-FL and Co_3O_4-C catalysts.

Based on the quantitative analysis, the Co^{2+}/Co^{3+} molar ratio of the two catalysts was Co_3O_4-FL (1.46) > Co_3O_4-C (1.31). The higher molar ratio of Co^{2+}/Co^{3+} than Co_3O_4-FL indicates that a higher abundance of Co^{2+} cations was presented on the surface of Co_3O_4-FL, which could manifest an increased redox activity for methane oxidation [28]. This trend is in good agreement with that of low-temperature reducibility. According to the quantitative analysis of the O 1s spectra, the O_{sur}/O_{latt} malor ratio of Co_3O_4-FL (0.50) is similar to that of Co_3O_4-C (0.51), whereas Co_3O_4-FL can provide other active sites for the surface oxygen species and boost the catalytic activity.

3.2. Methane Catalytic Oxidation

The effect of methane oxidation on Co_3O_4-FL and Co_3O_4-C catalysts is depicted in Figure 6. It seems that the activity is influenced by the different morphologies. The temperatures for the 50% conversion of methane (T_{50}) and 90% conversion of methane (T_{90}) in Co_3O_4-FL are 380 and 430 °C, respectively, which are much lower than these temperature values for Co_3O_4-C at the same conversion rate. This can be explained by the relatively high specific surface area, the greater number of active surface oxygen species, and the higher reducibility of highly exposed Co_3O_4-FL. Interestingly, Co_3O_4-FL showed nearly identical T_{50} and T_{90} values in the first three recycles, indicating the robust catalytic stability of Co_3O_4-FL. Meanwhile, other thermal stability tests were carried out at T_{50}, T_{80} and T_{100} under the same catalytic conditions (Figure 7). The values of T_{50}, T_{80} and T_{100} within the 20 h tests were 380, 415, and 520 °C, respectively, without variation. This result confirms that Co_3O_4-FL has excellent thermal stability, suggesting its great potential practical applicability.

Based on the previous characterizations and test results, the catalytic methane oxidation of Co_3O_4-FL can be enacted via a suprafacial mechanism, whereby the dissociatively adsorbed surface oxygen and the surface lattice oxygen act as the reaction active species. Besides this, the role of the reactive {112} plane in the Co_3O_4 nanosheets, and the oxygen vacancies derived from the mobility of lattice oxygen after the surface oxygen is consumed during methane oxidation, appear to be necessary.

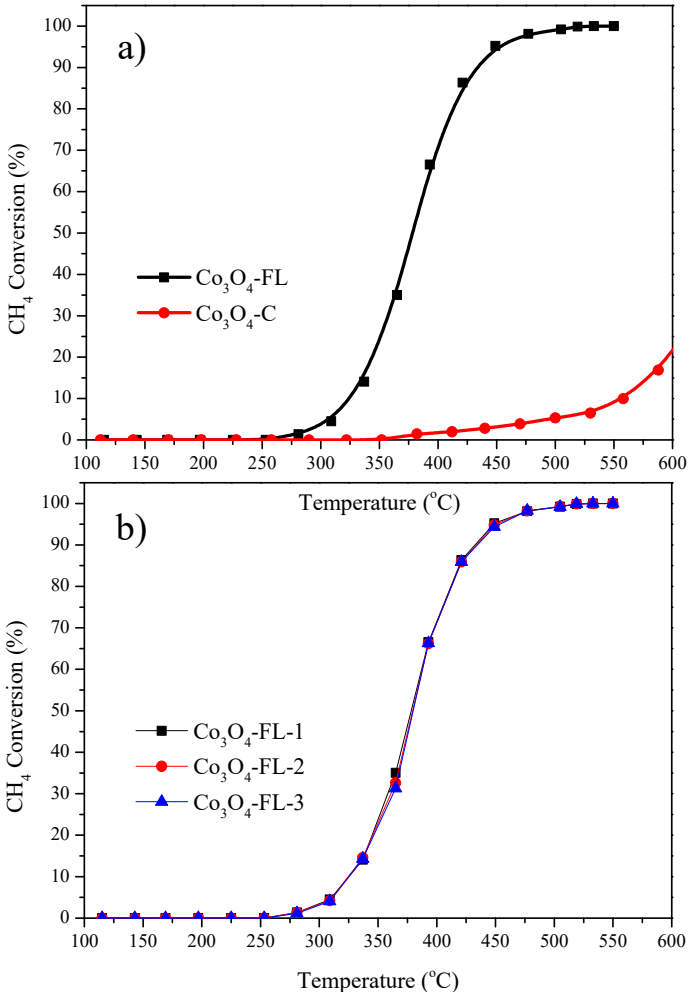

Figure 6. The light-off curves of CH_4 oxidation as a function of reaction temperature over the Co_3O_4-FLcatalysts (**a**) and the catalytic stability of Co_3O_4-FLcatalysts (**b**) (reactant composition of 2% CH_4, 20% O_2, air balanced, WHSV = 21,000 mL g^{-1} h^{-1}).

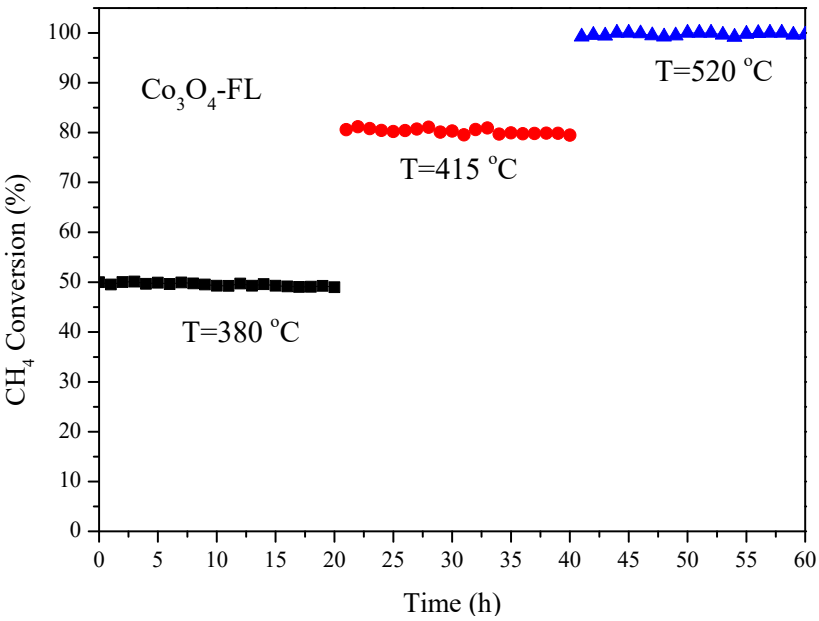

Figure 7. The catalytic stability of CH_4 oxidation over Co_3O_4-FLcatalysts at T_{50}, T_{80} and T_{100}, respectively.

4. Conclusions

In this study, flower-like Co_3O_4 hierarchical microspheres composed of nanosheets were prepared via a solvothermal method for methane oxidation. The dominantly exposed {112} crystal planes, together with the desorption of higher levels of active surface oxygen and the active species of lattice oxygen, lead to the presence of more active sites for C–H bond-breaking, which boosted the methane oxidation activity to a T_{90} of 430 °C at 21,000 mL g^{-1} h^{-1}. These results provide guidance for the design and preparation of non-noble metal catalysts for methane oxidation and other oxidative reactions.

Author Contributions: Conceptualization, C.L.; data curation, J.Z.; formal analysis, D.D. and Y.H.; project administration, C.W. and M.L.; resources, J.G. and Y.Q.; supervision, C.L.; writing—original draft, C.W.; writing—review & editing, C.L. and M.L. funding acquisition, C.L., C.W. and M.L. All authors have read and agreed to the published version of the manuscript.

Funding: This work was supported by National Natural Science Foundation of China (NSFC) (21978003), Key Research Project of Natural Science in Universities of Anhui Province (No. KJ2019ZD62, No. KJ2019A0850, No. KJ2020A0749), Excellent Young Talents Foundation in Universities of Anhui Province (gxyq2021223), and Natural Science Foundation of Shandong Province (ZR2020QB139).

Institutional Review Board Statement: Not applicable.

Informed Consent Statement: Not applicable.

Data Availability Statement: All the data is available within the manuscript.

Acknowledgments: This research was supported in part by Engineering Technology Research Center of Silicon-based Materials (Anhui) and Functional Powder Materials Laboratory of Bengbu.

Conflicts of Interest: The authors declare no conflict of interest.

References

1. Kamal, M.S.; Razzak, S.A.; Hossain, M.M. Catalytic oxidation of volatile organic compounds (VOCs)—A review. *Atmos. Environ.* **2016**, *140*, 117–134. [CrossRef]
2. Fletcher, S.E.M.; Schaefer, H. Rising methane: A new climate challenge. *Science* **2019**, *364*, 932–933. [CrossRef] [PubMed]
3. Vickers, S.M.; Gholami, R.; Smith, K.J.; MacLachlan, M.J. Mesoporous Mn- and La doped cerium oxide/cobalt oxide mixed metal catalysts for methane oxidation. *Appl. Mater. Interfaces* **2015**, *7*, 11460–11466. [CrossRef] [PubMed]
4. Liu, W.; Xiang, W.; Guan, N.; Cui, R.; Cheng, H.; Chen, X.; Song, Z.; Zhang, X.; Zhang, Y. Enhanced catalytic performance for toluene purification over Co_3O_4/MnO_2 catalyst through the construction of different Co_3O_4-MnO_2 interface. *Sep. Purif. Technol.* **2022**, *278*, 119590. [CrossRef]
5. Yu, Q.; Wang, C.; Li, X.; Li, Z.; Wang, L.; Zhang, Q.; Wu, G.; Li, Z. Engineering an effective MnO_2 catalyst from $LaMnO_3$ for catalytic methane combustion. *Fuel* **2019**, *239*, 1240–1245. [CrossRef]
6. Yu, Q.; Liu, C.; Li, X.; Wang, C.; Wang, X.; Cao, H.; Zhao, M.; Wu, G.; Su, W.; Ma, T.; et al. N-doping activated defective Co_3O_4 as an efficient catalyst for low-temperature methane oxidation. *Appl. Catal. B* **2020**, *269*, 118757. [CrossRef]
7. Sanchis, R.; García, A.; Ivars-Barceló, F.; Taylor, S.H.; García, T.; Dejoz, A.; Vázquez, M.I.; Solsona, B. Highly active Co_3O_4-based catalysts for totaloxidation of light C1–C3 alkanesprepared by a simplesoft chemistry method: Effect of the heat-treatment temperature and mixture of alkanes. *Materials* **2021**, *14*, 7120. [CrossRef]
8. Choya, A.; de Rivas, B.; Gutiérrez-Ortiz, J.I.; López-Fonseca, R. Bulk Co_3O_4 for methane oxidation: Effect of the synthesis route on physico-chemical properties and catalytic performance. *Catalysts* **2022**, *12*, 87. [CrossRef]
9. Yu, Q.; Zhuang, R.; Gao, W.; Yi, H.; Xie, X.; Zhang, Y.; Tang, X. Mesoporous Co_3O_4 with large specific surface area derived from MCM-48 for catalytic oxidation of toluene. *J. Solid State Chem.* **2022**, *307*, 122802. [CrossRef]
10. Miao, L.; Tang, X.; Zhao, S.; Xie, X.; Du, C.; Tang, T.; Yi, H. Study on mechanism of low-temperature oxidation of n-hexanal catalysed by 2D ultrathin Co_3O_4 nanosheets. *Nano Res.* **2022**, *15*, 1660–1671. [CrossRef]
11. Wang, X.; Chen, X.; Gao, L.; Zheng, H.; Zhang, Z.; Qian, Y. One-Dimensional Arrays of Co_3O_4 Nanoparticles: Synthesis, Characterization, and Optical and Electrochemical Properties. *J. Phys. Chem. B* **2004**, *108*, 16401–16404. [CrossRef]
12. Hu, L.; Peng, Q.; Li, Y. Selective synthesis of Co_3O_4 nanocrystal with different shape and crystal plane effect on catalytic property for methane combustion. *J. Am. Chem. Soc.* **2008**, *130*, 16136–16137. [CrossRef]
13. Liotta, L.F.; Wu, H.; Pantaleo, G.; Venezia, A.M. Co_3O_4 nanocrystals and Co_3O_4–MO_x binary oxides for CO, CH_4 and VOC oxidation at low temperatures: A review. *Catal. Sci. Technol.* **2013**, *3*, 3085–3102. [CrossRef]
14. Fei, Z.; He, S.; Li, L.; Ji, W.; Au, C.T. Morphology-directed synthesis of Co_3O_4 nanotubes based on modified Kirkendall effect and its application in CH_4 combustion. *Chem. Commun.* **2012**, *48*, 853–855. [CrossRef] [PubMed]

15. Setiawan, A.; Kennedy, E.M.; Dlugogorski, B.Z.; Adesina, A.A.; Stockenhuber, M. The stability of Co_3O_4, Fe_2O_3, Au/Co_3O_4 and Au/Fe_2O_3 catalysts in the catalytic combustion of lean methane mixtures in the presence of water. *Catal. Today* **2015**, *258*, 276–283. [CrossRef]
16. Liu, S.; Liu, P.; Niu, R.; Wang, S.; Li, J. Facile synthesis of mesoporous Co_3O_4 nanoflowers for catalytic combustion of ventilation air methane. *Chem. Res. Chin. Univ.* **2017**, *33*, 965–970. [CrossRef]
17. Liu, Y.; Dai, H.; Du, Y.; Deng, J.; Zhang, L.; Zhao, Z.; Au, C.T. Controlled preparation and high catalytic performance of three-dimensionally ordered macroporous $LaMnO_3$ with nanovoid skeletons for the combustion of toluene. *J. Catal.* **2012**, *287*, 149–160. [CrossRef]
18. Cai, T.; Huang, H.; Deng, W.; Dai, Q.; Liu, W.; Wang, X. Catalytic combustion of 1,2-dichlorobenzene at low temperature over Mn-modified Co_3O_4 catalysts. *Appl. Catal. B* **2015**, *166*, 393–405. [CrossRef]
19. Konsolakis, M.; Sgourakis, M.; Carabineiro, S.A.C. Surface and redox properties of cobalt-ceria binary oxides: On the effect of Co content and pretreatment conditions. *Appl. Surf. Sci.* **2015**, *341*, 48–54. [CrossRef]
20. Barreca, D.; Massignan, C.; Daolio, S.; Fabrizio, M.; Piccirillo, C.; Armelao, L.; Tondello, E. Composition and microstructure of cobalt oxide thin films obtained from a novel cobalt (II) precursor by chemical vapor deposition. *Chem. Mater.* **2001**, *13*, 588–593. [CrossRef]
21. Wei, W.; Chen, W.; Ivey, D.G. Rock salt—Spinel structural transformation in anodically electrodeposited Mn−Co−O nanocrystals. *Chem. Mater.* **2008**, *20*, 1941–1947. [CrossRef]
22. Biesinger, M.C.; Payne, B.P.; Grosvenor, A.P.; Lau, L.W.M.; Gerson, A.R.; Smart, R.S.C. Resolving surface chemical states in XPS analysis of first row transition metals, oxides and hydroxides: Cr, Mn, Fe, Co and Ni. *Appl. Surf. Sci.* **2011**, *257*, 2717–2730. [CrossRef]
23. Díaz-Fernández, D.; Méndez, J.; Bomatí-Miguel, O.; Yubero, F.; Mossanek, R.J.O.; Abbate, M.; Domínguez-Cañizares, G.; Gutiérrez, A.; Tougaard, S.; Soriano, L. The growth of cobalt oxides on HOPG and SiO_2 surfaces: A comparative study. *Surf. Sci.* **2014**, *624*, 145–153. [CrossRef]
24. Lykhach, Y.; Faisal, F.; Skála, T.; Neitzel, A.; Tsud, N.; Vorokhta, M.; Dvořák, F.; Beranová, K.; Kosto, Y.; Prince, K.C.; et al. Interplay between the metal-support interaction and stability in Pt/Co_3O_4 (111) model catalysts. *J. Mater. Chem. A* **2018**, *6*, 23078–23086. [CrossRef]
25. Chen, J.; Shi, W.; Yang, S.; Arandiyan, H.; Li, J. Distinguished roles with various vanadium loadings of $CoCr_{2-x}V_xO_4$ (x = 0–0.20) for Methane Combustion. *J. Phys. Chem. C* **2011**, *115*, 17400–17408. [CrossRef]
26. Gautier, J.L.; Rios, E.; Gracia, M.; Marco, J.F.; Gancedo, J.R. Characterisation by X-ray photoelectron spectroscopy of thin $MnxCo_{3-x}O_4$ ($1 \geq x \geq 0$) spinel films prepared by low-temperature spray pyrolysis. *Thin Solid Film.* **1997**, *311*, 51–57. [CrossRef]
27. Valeri, S.; Borghi, A.; Gazzadi, G.C.; Di Bona, A. Growth and structure of cobalt oxide on (001) bct cobalt film. *Surf. Sci.* **1999**, *423*, 346–356. [CrossRef]
28. Yuan, C.; Liu, S.Y.; Wang, Z.Q.; Wang, G.Y. Catalytic oxidation of low concentrations of vinyl chloride over spinel-type Co_3O_4 catalysts. *React. Kinet. Mech. Catal.* **2018**, *125*, 757–771. [CrossRef]